Int. J. Heat Mass Transfer. Vol. 29, No. 11, pp. 1683–1694, 1986
Printed in Great Britain

0017–9310/86 $3.00 + 0.00
Pergamon Journals Ltd.

Thermally induced hygroscopic mass transfer in a fibrous medium

DAVID A. PIERCE and STEVE M. BENNER*

Drexel University, Department of Chemical Engineering, 32nd and Chestnut Streets, Philadelphia, PA 19104, U.S.A.

(*Received* 18 *December* 1985 *and in final form* 12 *March* 1986)

Abstract—A fiberglass sample was used to study the hygroscopic mass transfer produced by a temperature difference across a moist, fibrous medium. Humidity probes and thermocouples were implanted in the sample and used to continuously monitor changes in the relative humidity and temperature as a result of the moisture migration. The effects of average temperature, thermal gradient magnitude and average moisture content were some of the parameters studied. The data was analyzed using a mechanistic analogy to the irreversible thermodynamic model. Vapor and liquid fluxes were evaluated along with vapor and liquid conductivities. The phenomenological coefficients associated with the liquid and vapor fluxes were calculated, and the flux contributions due to the thermal and concentration gradients were determined for steady-state conditions. Transient data for the humidity, temperature and moisture content were also either measured or calculated.

INTRODUCTION

THE PHENOMENON of moisture migration due to a thermal gradient has been studied extensively by many researchers in many different ways. Some examples are studies on soil moisture migration due to cylindrical heat sources such as pipes and wires, on drying processes including food, wood and concrete, and on moisture migration through fibrous and porous materials such as insulations. Insulations have been receiving more attention recently due to the increasing concern about energy efficiency. Since moisture migration increases the effective heat conductivity of materials, a basic understanding of the relationship between heat and mass transfer should lead to methods which increase energy efficiency and thus reduce the cost of heating and cooling.

Mass transfer due to a thermal gradient occurs when a system experiences a change in temperature at a point or boundary of the system. Heat is transferred by the evaporation, vapor and liquid diffusion, and condensation of moisture inside the material. Since this thermal mass transfer can be significant, it must be considered in any nonisothermal mass transfer operation. Certainly large thermal gradients must be taken into consideration when studying the mass transfer which occurs in insulating materials and during drying.

This research will investigate the effect of a temperature difference on the moisture transfer and distribution in fiberboard insulation. The research will concentrate on hygroscopic moisture content since at these low moisture contents capillary and gravitational effects are minimal. There are inadequate experimental data for characterizing moisture as it moves through fibrous materials and even less for low moisture contents. Transient and steady-state data were gathered to help in the identification of the proper mechanisms of thermal moisture migration in isolated fibrous materials. The concepts developed here should lead to a more basic understanding of moisture migration as a result of a temperature gradient in any porous or fibrous system.

The phenomenon of simultaneous heat and mass transfer has been studied and discussed in the literature since the early 1900s. Moisture will migrate through a porous body as a result of molecular diffusion, pressure gradients, gravity, capillary action, vapor pressure gradients and thermal gradients. Initially, the effect of a thermal gradient on moisture migration was neither recognized nor quantified in any way. During the mid-1900s, this effect was studied in depth by A. V. Luikov. Luikov quantified the relationship between heat and mass transfer based on the energy and mass balances in a porous body [1]. Using the concepts from irreversible thermodynamics, Luikov showed that mass potential is the driving force for mass transfer in porous bodies [2]. The mass potential for mass transfer is equivalent to temperature for heat transfer. Luikov summarized the basic equations and theory developed mostly by Russian scientists during the mid-1900s in a review article in 1975 [3]. This laid the fundamental basis for most of the research which has been done since.

Simultaneous heat and mass transfer theory has applications in many fields. Examples include moisture migration in soils [4–6], insulation [7], foods [8] and concrete [9]. Soils, concrete and foods generally have boundaries through which moisture passes while

* To whom correspondence should be addressed.

NOMENCLATURE

AH	absolute humidity
a	porosity
D	diffusivity
H	fractional relative humidity
J	flux
K	mass transport conductivity
L	phenomenological coefficient
MC	moisture content on a dry basis
P, P_v	total pressure, partial pressure
R	universal gas constant
T	temperature
X	driving force, thermodynamic force.

Greek symbols

ε	tortuosity factor
λ	thermal conductivity
μ	chemical potential
ρ	density
ψ	water potential gradient
δ	thermogradient coefficient.

Subscripts

a	air
i, j, k	indices
l	liquid
0	initial, equilibrium
q	heat
t	temperature, thermal
v	vapor
w	water.

insulations often have impervious boundaries. To bridge the gap between the mathematical theory and the experimental systems, the physical constants and thermodynamic parameters of the system must be measured or estimated. Many institutions such as ASHRAE and ASTM contribute to the evaluation of physical constants such as density, mean fiber size, porosity, mean specific surface area and percent bonding material, and parameters such as the normal and thermal mass transfer coefficients and diffusivities. In this way, all the various applications and types of systems are linked into one coherent data base which can apply to any system.

The system of interest is a hygroscopic fibrous material which has boundaries that are impervious to moisture flow. Eckert and Faghri experimentally studied a hygroscopic closed system of sand and developed a model of their system using a mechanistic approach [4]. They assumed that the thermodynamic and transport properties of the system were constant. They accurately predicted the drying-out time and moisture distribution in a sand sample as a function of Luikov and Fourier numbers. In addition, the thermal mass transfer coefficient (also referred to as the thermogradient coefficient) was investigated. More recently, Thomas *et al.* experimentally studied fiberglass insulation [7]. They measured transient and steady-state moisture and temperature profiles of saturated fibrous insulation. Although this experimental system is similar, the range of moisture contents studied is two orders of magnitude greater than this study and out of the hygroscopic range. This greatly limits the comparison of the two studies. Also, the moisture contents were determined gravimetrically by periodically weighing each slice of the sample. Even though the procedure was performed quickly, the temperature gradient had to be re-established after each weighing and a small moisture loss certainly occurred. These interruptions may limit the experimental transient conclusions which can be drawn. Finally, Thomas *et al.* base their mathematical model on the assumption that all moisture migrates in the vapor phase. This has been shown by many investigators to be too simplistic to accurately model the system. On the other hand, Fortes and Okos developed a comprehensive set of heat and mass transfer equations for hygroscopic moisture transfer [6]. The proposed model uses the theories of irreversible thermodynamics as a basis to derive the fundamental transport equations. They point out that the assumption that all the moisture migrates in one dominating mechanism is too simplistic and leads to inaccurate results. They state that the driving forces for heat and mass transfer in the liquid and vapor phases are a combination of the temperature and equilibrium relative humidity. The model was verified experimentally using sand and later using extruded corn meal [8]. This theory will be applied to the hygroscopic fiberglass insulation used in this study.

Since temperature and relative humidity have been verified as possible driving forces for simultaneous heat and mass transfer, measurement of the temperature and relative humidity gradients will be made. Although thermal gradients are routinely measured, relative humidity measurements have not been made directly. Fortes and Okos base their complete analysis of the heat and mass transfer on temperature measurements and equilibrium moisture data. In this project, the temperature and relative humidity were measured directly and, from these data and the appropriate model, the transient and steady-state moisture content and absolute humidity gradients were calculated. Finally, based on the moisture content and absolute

humidity gradients, the relative importance of the vapor and liquid diffusion can be calculated.

This research project centered on the transient and steady-state transfer characteristics of a fiberglass insulation with moisture contents in the hygroscopic range. There were five main objectives of the project: (1) to measure directly relative humidity profiles within the sample using relative humidity probes; (2) to quantify the response of the sample to a step change in boundary temperatures; (3) to determine the effect of average temperature, temperature difference and moisture content on the response; (4) to utilize current theory to calculate the transport fluxes and parameters associated with hygroscopic moisture transfer; and (5) to determine the relative importance of the various transport mechanisms.

THEORY

The following theory is based on work by Fortes and Okos [6, 8]. The theories of irreversible thermodynamics outline the driving forces for heat and mass transfer; however, since the phenomenological coefficients derived in the irreversible thermodynamics model are unknown, the final forms of the equations will be derived through a mechanistic approach. Thus, the model derived is a mechanistic approach based upon irreversible thermodynamics.

In the 1920s, L. Onsager developed a systematic approach to modeling irreversible processes. Although Onsager's theorem will not be rigorously proved here, it is available in *Physics Review* **37** (1931) and **38** (1931). Essentially, Onsager states that irreversible phenomena are caused by thermodynamic 'forces', X_i, such as temperature and concentration gradients, gravity and electric potential. These forces cause fluxes, flows, or currents, J_i. Onsager stated that any thermodynamic force can cause any flow and that they are related by symmetrical phenomenological coefficients, L_{ij}

$$J_i = \sum L_{ij} X_i. \tag{1}$$

Therefore, any flow is caused by the combination of all acting forces. For a single component system with transport in the liquid and vapor phases, the general equations for heat and mass transfer can be written as:

$$J_q = L_{qq}X_q + L_{ql}X_l + L_{qv}X_v \tag{2}$$

$$J_l = L_{lq}X_q + L_{ll}X_l + L_{lv}X_v \tag{3}$$

$$J_v = L_{vq}X_q + L_{vl}X_l + L_{vv}X_v. \tag{4}$$

Since the effects of gravity on mass transfer are negligible for a hygroscopic system, the final driving forces are

$$X_q = -(1/T^2)(\nabla T) \tag{5}$$

$$X_l = -(1/T)(\nabla \mu_l)_t \tag{6}$$

$$X_v = -(1/T)(\nabla \mu_v)_t. \tag{7}$$

Since the vapor and liquid phases are in equilibrium with each other, the chemical potential, μ, of the liquid and vapor phases must be equal; therefore, the driving forces for liquid and vapor transport are equal. Redefining the chemical potential in terms of the relative humidity, H, equations (2)–(4) become

$$J_q = -(L_{qq}/T^2)(\nabla T) - (L_{ql} + L_{qv})(R/H)(\nabla H)_t \tag{8}$$

$$J_l = -(L_{lq}/T^2)(\nabla T) - (L_{ll} + L_{lv})(R/H)(\nabla H)_t \tag{9}$$

$$J_v = -(L_{vq}/T^2)(\nabla T) - (L_{vl} + L_{vv})(R/H)(\nabla H)_t. \tag{10}$$

The driving forces for heat transfer and vapor and liquid diffusion are therefore the equilibrium relative humidity and temperature gradients. Since the phenomenological coefficients are unknown at this point, no further development is possible without analogy to a mechanistic approach.

For the mechanistic approach, the vapor flux, J_v, is assumed to be occurring by diffusion caused by a vapor concentration gradient and is described by

$$J_v = -k_v \nabla \rho_v \tag{11}$$

where the vapor conductivity, k_v, is

$$k_v = -[\varepsilon a P/(P - P_v)]D_w \tag{12}$$

and is a function of the tortuosity, ε, porosity, a, water diffusivity in air, D_w, and the vapor pressure gradient (total pressure, P, minus the partial pressure, P_v). By defining the vapor pressure gradient in terms of the relative humidity and temperature and expanding the resulting expression, equation (11) now becomes the final form of the vapor flux equation

$$J_v = -k_v(\rho_{v0}\,\partial H/\partial T + H\,\mathrm{d}\rho_{v0}/\mathrm{d}T)(\nabla T) - k_v\rho_{v0}(\nabla H)_t. \tag{13}$$

Similarly the liquid flux, J_l, can be defined by a modified form of Darcy's law:

$$J_l = -\rho_l k_l \nabla \psi \tag{14}$$

where ψ is the gradient of water potential, ρ_l is the liquid density and k_l is the liquid conductivity. The water potential is a combination of the gravimetric water potential, the osmotic water potential and the matric water potential. Since the effect of gravity in the hygroscopic range is negligible, the total water potential includes only the osmotic and matric water potentials and can be defined in terms of the relative humidity and temperature. Equation (14) then becomes

$$J_l = -\rho_l k_l R[\ln(H)(\nabla T) + (T/H)(\nabla H)]. \tag{15}$$

Therefore, equations (13) and (15) represent the vapor and liquid fluxes using temperature and equilibrium relative humidity as driving forces.

The phenomenological coefficients can be defined by comparing equation (13) to equation (10) and equation (15) to equation (9). To do this, Onsager's

reciprocal relationship is used. Also, in order to determine L_{qq}, Fourier's law is used to define the heat transfer process due to conduction as follows:

$$J_q = -\lambda_t \nabla T \tag{16}$$

where λ_t is the apparent thermal conductivity. By comparing equation (16) with equation (8), the following is obtained:

$$L_{qq} = T^2 \lambda_t. \tag{17}$$

From equation (9) and equation (15)

$$L_{lq} = \rho_l k_l R T^2 \ln(H) \tag{18}$$

and

$$L_{ll} + L_{lv} = \rho_l k_l T. \tag{19}$$

And, by comparing equation (10) with equation (13), the remaining coefficients can be evaluated:

$$L_{vq} = T^2 k_v (\rho_{v0} \partial H/\partial T + H \, d\rho_{v0}/dT) \tag{20}$$

and

$$L_{vl} + L_{vv} = k_v \rho_{v0} H/R. \tag{21}$$

The final form of the heat flux can now be written using the Onsager relationship:

$$J_q = -\lambda_t(\nabla T) - [\rho_l k_l R \ln(H) + k_v(\rho_{v0} \partial H/\partial T + H \, d\rho_{v0}/dT)](RT^2/H)(\nabla H)_t. \tag{22}$$

Equations (13), (15) and (22) are the final forms of the energy and mass transport equations.

From a mass balance at steady state, the net flux of water into any point must be zero, therefore:

$$J_l + J_v = 0. \tag{23}$$

Knowing the vapor diffusivity, the vapor conductivity can be calculated using equation (12). The following relationship from Fortes and Okos is used to calculate the saturated vapor density:

$$\rho_{v0} = (2.54 \times 10^8)/T \times \exp(-5200/T). \tag{24}$$

The vapor flux can be calculated using equation (13) and, finally, the liquid conductivity, k_l, can also be calculated from equations (15) and (23). By coupling the temperature and relative humidity measurements to the vapor diffusivity, the fluxes for the vapor and liquid phases and their respective mass conductivities can be determined.

Equilibrium moisture contents of two samples of fiberboard insulation were obtained by Luu [10]. The physical properties of the sample are shown in Table 1. Since the adsorption isotherm is unsteady and only valid after the sample has been completely dried, the desorption isotherm more accurately represents the changes in moisture content as a function of relative humidity and temperature. The desorption isotherms are shown in Fig. 1.

Table 1. Specification of glass fiberboard sample

Dry density, kg m^{-3}	101
Porosity, m^3 m^{-3}	0.954
Mean fiber size, mm	0.0116
Mean specific surface, m^2 m^{-3}	16,000
Percent bonding, wt%	10.7

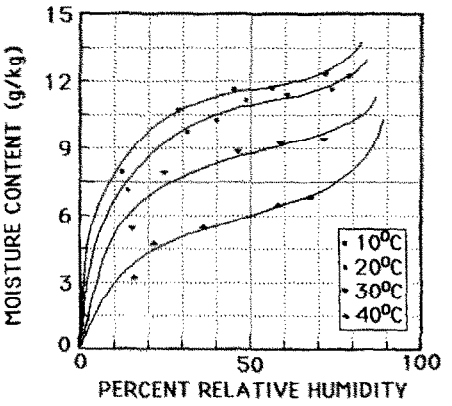

FIG. 1. Desorption isotherms for 101 kg m^{-3} density glass fiberboard.

The desorption data was modeled based upon the experimental work presented in Luu's thesis. The data were fitted with a set of polynomials using a statistical analytical program. The data were divided into two sections, and two polynomials were used to fit the data with correlation coefficients of 0.98. For relative humidities between 0 and 90%, the following equation applies, as calculated by the nonlinear polynomial regression routine:

$$MC = -0.6342 - 0.045544(T) - 0.022318(H)(T) + 0.36557(T)^{1/2} + 1.82204(H)^{1/2} - 0.32887(H)^3. \tag{25}$$

For relative humidities above 90%, the following equation applies:

$$MC = 640.2452 - 0.054375(T) - 3336.6287(H) + 9.77 \times 10^{-4}(T)^2 + 6475.5887(H)^2 - 5535.465(H)^3 + 1759.895(H)^4 \tag{26}$$

H is the fractional relative humidity, T is the temperature in °C, and MC is the weight percent of moisture content. Using this model, the moisture content within the fiberglass sample at any position, time, temperature, and relative humidity can be calculated.

A computer model of the psychrometric chart was developed from equations presented by Pallady and Hanley [12] and is used to calculate the absolute humidity within the sample. The model is based on the Van der Waals equation with a temperature-

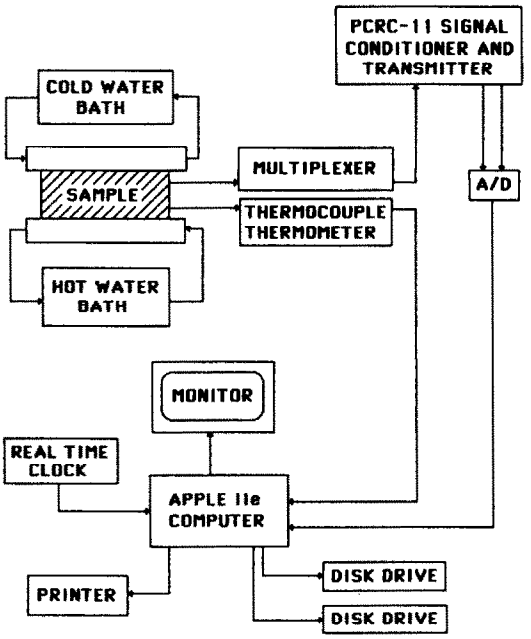

FIG. 2. Experimental equipment schematic.

dependent constant. The model was checked for accuracy using the psychrometric chart with excellent results. Absolute humidities were within 0.01% kg moisture/kg dry air. This is certainly accurate enough for the data obtained.

EXPERIMENTAL EQUIPMENT, PROCEDURE AND CONDITIONS

The transient and steady-state thermal mass transfer characteristics were the objectives of this research. Therefore, the equipment was designed to continuously monitor the system variables of temperature and relative humidity. The experimental system was designed to exhibit the following characteristics:

1. Maintain a constant overall average moisture content.
2. Expose the sample to temperatures between 0 and 35°C.
3. Continuously monitor temperature in the sample.
4. Continuously monitor relative humidity in the sample.
5. Minimize lateral end effects.

Figure 2 is a schematic of the overall equipment layout, and Fig. 3 is an expanded side view of the sample chamber. The following is a description of each section of the equipment.

Temperature gradients were imposed on the sample using two circulating water baths. The top bath, used for the cold side, uses on/off control for the heating and cooling coils. An ethylene glycol/water solution was used in the bath to obtain temperatures near 0°C. The coolant entered the Plexiglass chamber and contacted the 0.13-cm-thick aluminum plate on top of the sample. The bottom bath also used on/off control and pumped the tempered water into the bottom Plexiglass chamber where it contacted the bottom aluminum plate. Using these two baths, a temperature gradient could be imposed on the sample for extended periods of time.

The sample chamber consisted of 0.6-cm-thick Plexiglass walls that were 5 cm wide by 30 cm long (Fig. 3). The four walls were attached to the top and bottom aluminum plates using screws and silicon sealant. The sealant ensured that no moisture could migrate into or out of the sample during the run. Four small holes were drilled into the right side of the sample chamber for the four relative humidity sensors and the type-T thermocouples. The chamber was designed to accommodate a sample which was sliced into five sections. Four relative humidity sensors and four thermocouples were placed between the five sections while the final two thermocouples are placed on the top and bottom of the sample next to the aluminum plates. This design permitted four internal relative humidity and temperature measurements to be made along with the top and bottom plate temperatures. The wires were sealed into the holes using the silicon sealant once the sensors were in place. This provided a totally isolated sample which could be externally monitored using implanted sensors.

The six type-T thermocouples interface with the computer using a thermocouple thermometer and analog card. The thermocouple thermometer had a built in electronic ice point and a reference voltage which made the unit self-sufficient. A temperature was obtained by selecting the desired channel; then reading the temperature into the computer's memory. In this manner, any of the six thermocouples could be read at any time.

The relative humidity is proportional to the impedance output of the relative humidity sensor. Since the relative humidity sensors must not come into contact with liquid water, they were protected with a 0.5 μm semi-permeable membrane. This membrane permits water vapor to freely pass through the sensor while prohibiting liquid water from contacting the sensor. The sensor dimensions were $1.3 \times 2.5 \times 0.16$ cm which made them small enough to fit between the sample slices. The sensor area represented only 0.36% of the total transfer area (30.5×30.5 cm) and 3.2% of the test area (10×10 cm). Since this cross-sectional area was so small and the sensor positions were staggered, the sensors were assumed to be no impediment to vapor or liquid movement. The sensors were precalibrated and accurate to $\pm 0.5\%$ relative humidity for a 0–100–0% excursion. Due to the expense of the signal conditioner and transmitter, the four relative humidity sensors were interfaced through a multiplexor. Therefore, all four relative humidity sensors could use one signal conditioner/transmitter. Since

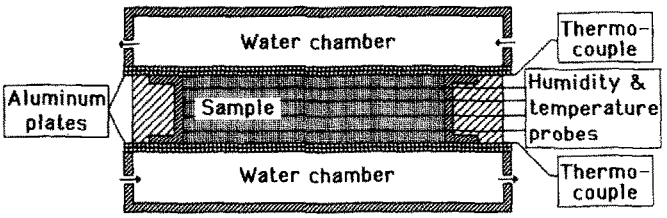

FIG. 3. Sample test assembly.

relative humidity is temperature dependent, the signal conditioner supplied two analog outputs: one for relative humidity and one for temperature. These two channels were read by the computer whenever desired using an analog-to-digital converter. Finally, the computer calculated the actual relative humidity inside the sample based on the actual temperature inside the sample and the sensor output.

The computer system collected, stored and printed all the data for each run. The system included two floppy disk drives, a monochrome monitor, a dot matrix printer and a real time clock. The software used this equipment to archive the data on floppy disks and on paper using the printer. As described, the complete system consisted of an undisturbed sample which was fully instrumented for temperature and relative humidity.

The sample chosen for this experimentation was a $30.5 \times 30.5 \times 5$ cm sample of fiberglass fiberboard insulation. Table 1 is a list of the insulation properties. This insulation was selected because it had been used previously at Drexel University by Luu [10]. Thus, the physical properties and equilibrium moisture content data obtained in the earlier work could be applied to this work. The 5-cm-thick fiberglass sample was carefully sliced into five sections. The top and bottom slices were approximately 0.6 cm thick and the middle three sections were 1.25 cm thick. Small cavities were needed for placement of the relative humidity probes in order to insure good contact between the slices. These cavities were cut into the slices to space the relative humidity sensors and thermocouples at distances of 0.6, 1.9, 3.2 and 4.4 cm from the top plate. As mentioned earlier, the sensors were carefully placed so that no sensor had a second sensor directly above or below it to interfere with the measurements or moisture transfer. The sensors were carefully spaced in the central region of the sample at least 10 cm from the nearest chamber wall. This 10-cm region around the probes was used as an insulating barrier to reduce lateral end effects. This reduced the actual test area from 30.5×30.5 cm to 10×10 cm.

The effect of slicing the sample on the moisture transfer was assumed to be negligible. Since the slicing would have little effect on vapor transfer, the effect would have to be on the liquid transfer. At the low moisture contents used in the study, capillary and gravitational transport are not significant, and the liquid is mostly transfered by surface diffusion. As long as there is good contact between the slices, this diffusion should not be affected.

After the sample was prepared, it was inserted into the chamber layer by layer. As each layer was positioned, each sensor and thermocouple were carefully placed in the desired location. After the final slice was inserted and the thermocouple placed on top, the aluminum plate was screwed on top and sealed with silicon glue. This procedure was completed within 10 min so that the water content of the sample did not change significantly during the assembly. The seals were carefully checked and resealed if necessary to ensure a constant moisture content in the sample. Finally, the water bath was placed on top, and the sample was ready for a run.

The average moisture content was determined by weighing the sample after a set of runs. This value was only accurate to $\pm 0.2\%$ due to the inaccuracies of the balance used but could be confirmed by calculating the local moisture contents from humidity and temperature data. For gradients as much as $6°C\ cm^{-1}$, 0.16 cm is a temperature change of almost 1°C. Since the probes are placed no more accurately than ± 0.16 cm, the accuracy of the temperature measurements is $\pm 1°C$. Using a similar analysis, the accuracy of the relative humidity measurement is $\pm 2\%$.

Three variables were chosen to be studied: average moisture content, average temperature, and overall temperature gradient. Table 2 is the list of runs and their corresponding experimental conditions. The temperatures are nominal conditions since the water baths were not adjusted after the run was started. Runs 1–8 represent a two-level factorial designed to study the three variables. The ranges for the average moisture content, average temperature, and temperature difference were 0.6–2.0% by weight (%wt), 15–20°C, and 20–30°C, respectively. Runs 9 and 10 were aimed at investigating the smaller temperature difference of 10°C and the higher average temperature of 30°C. Finally, Run 11 was a repeat of the conditions used in Run 7 to show the repeatability of the transient data and to ensure that a blackout during Run 7 did not adversely affect the data. These 11 runs and 10 sets of experimental conditions comprise the experimental study.

DISCUSSION OF RESULTS

The results can be broken into two groups: steady-state and transient. The temperature and relative

Table 2. Experimental program run conditions

Run	Average moisture content (% wt)	Average temperature (°C)	Temperature difference (°C)
1	0.6	20	20
2	0.6	15	20
3	0.6	20	30
4	0.6	15	30
5	2.0	20	20
6	2.0	15	20
7	2.0	20	30
8	2.0	15	30
9	2.0	20	10
10	2.0	30	10
11	2.0	20	30

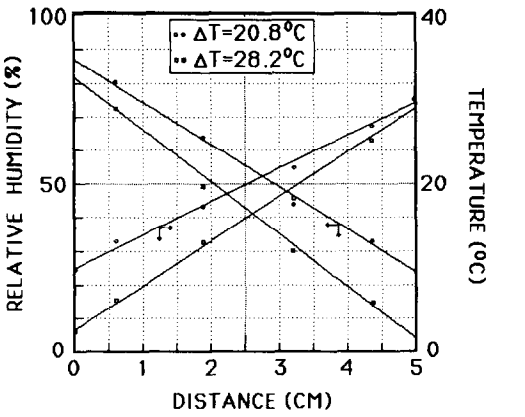

FIG. 4. Relative humidity distribution for an average moisture content of 0.6% wt.

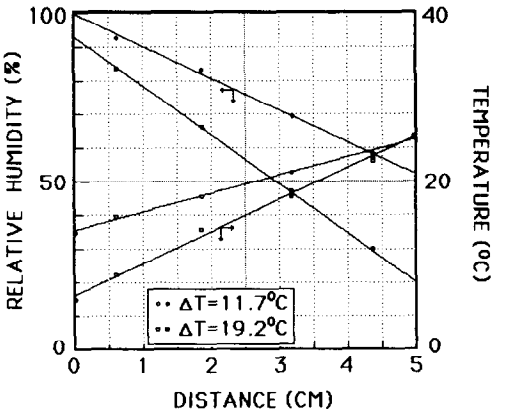

FIG. 5. Relative humidity distribution for an average moisture content of 2.0% wt.

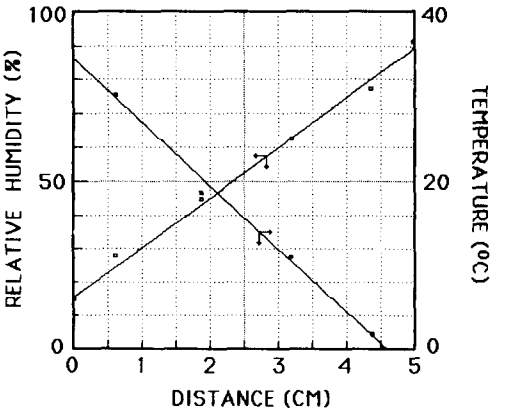

FIG. 6. Relative humidity distribution for an average moisture content of 2.0% wt and a temperature difference of 30.9°C.

humidity gradients were measured directly, and the moisture content and absolute humidity gradients were calculated from the measurements. One of the major objectives of this study was to determine the transient and steady-state changes in these gradients as a result of various average temperatures, temperature differences, and moisture contents.

Steady state

Figures 4–6 show the steady-state relative humidity and temperature distributions for five of the runs. The temperature distributions for the runs were approximately linear since the moisture content was too low to affect the thermal conductivity. Also as evident from the figures, the humidity distributions were essentially linear. The average temperature had no significant effect on either the relative humidity distribution or gradient (% cm^{-1}). The humidity gradients from runs with the same nominal temperature gradient and moisture contents (Runs 1–2 and 3–4 at 0.6% wt; 5–6, 7–8–11, and 9–10 at 2.0 %wt) were nearly identical in spite of their differences in average temperatures. As a result, only one run from each average temperature is shown in Figs. 4–6 (Runs 1, 4, 6, 7 and 9). An average temperature change of 25% resulted in a change of approximately 3% in the humidity gradient. This seemed to indicate that the average temperature does not affect the relative humidity gradient over the range of average temperatures studied. This implies that the transport parameters and constants are independent of temperature over the range 15–30°C.

On the other hand, the magnitude of the temperature difference does significantly affect the humidity gradient. Figures 4–6 show that the larger the temperature difference imposed on the sample the larger relative humidity gradient. An increase of 50% in the thermal gradient increased the opposing relative humidity gradient up to 30%. Since the direction of the thermal gradient is opposite to that of the relative humidity, it is logical that a larger thermal gradient induces a larger relative humidity gradient. This is also shown clearly by the vapor and liquid flux equations in the Theory section.

The effect of average moisture content on the relative humidity gradient can be determined by comparing runs with the same temperature difference and average temperature. A comparison of Runs 1 and 5

Table 3. Summary of results

Run	MC (% wt)	ΔT (°C)	ΔH (%)	ΔMC (% wt)	∇T (°C m^{-1})	∇H (m^{-1})	J_v (mg m^{-2} s^{-1})	k_v (cm^2 s^{-1})	k_l (10^{-15} s)	$\nabla MC/\nabla T$ (10^{-4} °C^{-1})
1	0.6	20.8	48.1	0.457	409	12.6	6.25	0.253	1.49	2.93
2	0.6	20.4	49.4	0.440	402	13.0	5.19	0.246	0.84	2.87
3	0.6	29.9	61.0	0.781	589	16.0	10.13	0.252	1.02	3.48
4	0.6	28.2	57.6	0.658	555	15.1	4.99	0.245	0.82	3.11
5	2.0	20.7	54.6	0.479	407	14.3	8.36	0.255	1.81	3.09
6	2.0	19.2	54.1	0.443	378	14.2	6.12	0.246	1.38	3.09
7	2.0	30.6	71.6	1.008	602	18.8	14.44	0.254	1.08	3.08
8	2.0	26.7	69.1	0.808	526	18.1	10.27	0.248	1.03	4.40
9	2.0	11.7	35.9	0.172	230	9.4	4.03	0.254	2.12	4.03
10	2.0	11.1	28.4	0.202	219	7.5	4.41	0.273	3.07	2.42
11	2.0	28.3	71.0	0.893	557	18.6	13.73	0.254	1.25	4.21

($\Delta T \approx 20$°C) and Runs 4 and 8 ($\Delta T \approx 30$°C) indicates that the runs with the higher average moisture content have a higher relative humidity gradient with all other conditions being equal. This effect was significantly smaller than that of the temperature difference. Of the three variables studied, the thermal gradient has the most significant effect on the relative humidity gradient. The larger the thermal gradient; the larger the relative humidity gradient. A higher average moisture content also increases the corresponding relative humidity gradient while the effect of average temperature is insignificant. The temperature, relative humidity, and moisture content differences for all 11 runs are listed in Table 3.

The moisture content was calculated at each point from the model of the equilibrium moisture content data (see Theory) and from the temperature and relative humidity measurements made during the run. Figure 7 shows the moisture distribution for Runs 5, 8 and 10 which all have an average moisture content of 2.0% wt. The average moisture content indicated by the figure is closer to 1% than 2%. This difference is due to the large amount of moisture near the cold plate which could not be measured by the top humidity sensor. When the sample slices were weighed, the moisture content of the slice near the cold side was greater than that indicated by the relative humidity sensor. Though it is not shown in the figure, there should be a rapid increase in moisture content as the distance approaches zero.

An analysis of moisture content, similar to that done for relative humidity, showed the effects of the three variables on the moisture distribution. The moisture distribution showed the same general behavior as that of the relative humidity. As with the relative humidity, the average temperature had little effect on the moisture content gradient, but the calculated moisture content at each point was higher for the lower average temperature. This implies that the greater the average temperature, the more drying out will occur in the lower and central area of the sample, with more of the moisture being driven to the cold plate region. Again, as with the relative humidity gradient, a larger thermal gradient induced a larger moisture content gradient. In addition, the distribution becomes more nonlinear with increasing temperature difference. Since the variables in front of the driving force terms in vapor and liquid flux equations are constant for a given set of conditions, a larger thermal gradient induces a larger relative humidity gradient and a larger moisture content gradient.

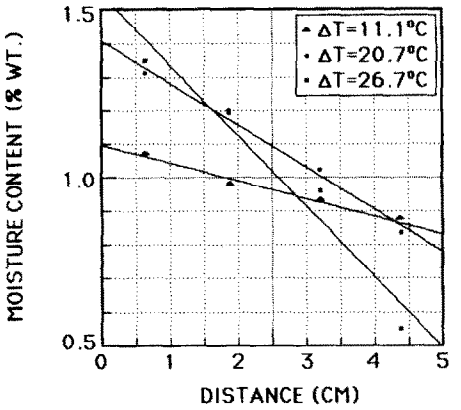

FIG. 7. Moisture distributions for an average moisture content of 2.0% wt.

An inspection of Table 3 also shows that the moisture content differences and therefore the moisture content gradients for Runs 5–8 are slightly larger than the gradients for Runs 1–4. This demonstrates that, to some extent, a larger average moisture content results in a greater moisture gradient.

The ratio of the moisture content gradient to the thermal gradient can be used to calculate the thermogradient coefficient. As can be seen in Table 3, the ratio ranges from about 2×10^{-4} to 4×10^{-4} °C^{-1} and increases with increasing thermal gradient. This coefficient was the phenomenological coefficient developed by Luikov to define thermal mass transfer in porous media [2]. The coefficient times the mass conductivity and the thermal gradient gives the mass transfer due to the thermal gradient. By inspection of equations (13) and (15), the vapor and liquid coefficients can be defined as

$$\delta_v = \rho_{v0}\,\partial H/\partial T + H\,\mathrm{d}\rho_{v0}/\mathrm{d}T \qquad (27)$$

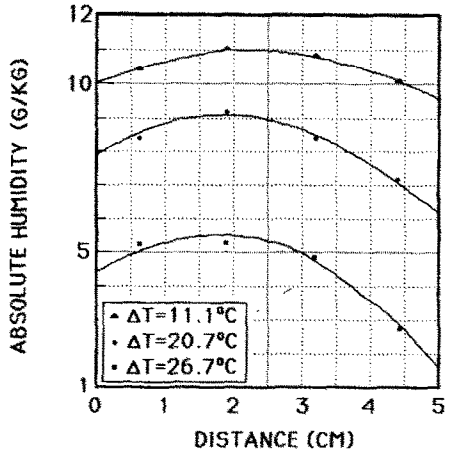

FIG. 8. Absolute humidity distributions for an average moisture content of 2.0% wt.

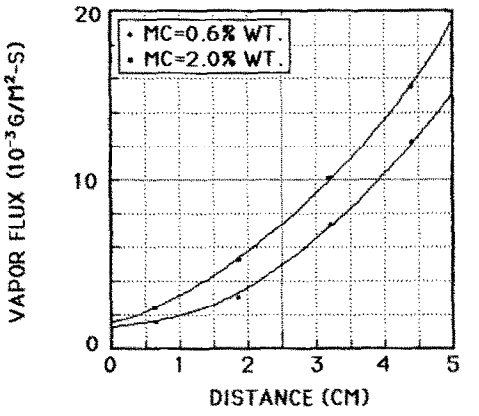

FIG. 9. Vapor flux distributions for an average temperature of 20°C and a temperature difference of 20.8°C.

$$\delta_l = \rho_l R \ln (H). \tag{28}$$

This coefficient has been dealt with extensively by Luikov and will not be discussed in detail here.

The final calculated variable was the absolute humidity (Fig. 8). The absolute humidity is the water vapor concentration of the air inside the sample. This may be the most difficult variable to analyze due to the nonlinear character of the psychrometric chart and the model presented earlier. However, in spite of any errors introduced, some obvious and significant observations can be made. First, a higher average temperature resulted in higher absolute humidities throughout the sample. Therefore, average temperature has a significant effect on the absolute humidity. Also, lower temperature differences resulted in higher absolute humidities but lower gradients in the sample (see Fig. 8). The absolute humidities for Runs 5–8 were slightly higher than the absolute humidities for Runs 1–4. Thus, the higher average moisture content in the sample results in higher absolute humidities in the sample.

By calculating the theoretical binary diffusivity for water and air, the vapor flux can be calculated using equation (13). Since at steady state the vapor flux is equal to the liquid flux as indicated by equation (23), the liquid mass conductivity, k_l, can also be calculated. The vapor and liquid mass conductivities were calculated at each measurement point in the sample; the average values of the mass conductivities, vapor fluxes, and relative humidity and temperature gradients are listed in Table 3. The point values for the vapor and liquid conductivities ranged between 0.23 and 0.30 $cm^2\ s^{-1}$ and 3.2×10^{-15} to 4.1×10^{-14} s, respectively. The liquid conductivity generally increased in the region of the warm plate, but this trend was not consistent. In addition, the liquid conductivity values were three orders of magnitude less than that predicted by Baladi for sand [13].

Figure 9 shows the vapor flux distributions for Runs 1 and 5 with average moisture contents of 0.6 and 2% wt, respectively, and both with average temperatures of 20°C and temperature differences of 20°C. The vapor flux increases as the hot plate is approached. As the liquid migrates toward the low moisture content region near the hot plate, it evaporates and diffuses back as vapor toward the cold plate where it condenses. This dynamic steady-state behavior is established slowly throughout the sample, and is maintained as long as energy is supplied to the system. The runs with the higher average temperature have higher vapor fluxes throughout the sample. Therefore, a larger thermal gradient causes a larger vapor flux through the sample. Equation (13) shows that a larger thermal gradient with all else constant would cause a larger vapor flux. Finally, Fig. 9 shows that the higher average moisture content in Run 5 has a higher vapor flux through the sample than the lower moisture content in Run 1.

The phenomenological coefficients for the liquid and vapor fluxes could now be calculated and used to estimate the mass transfer contributions due to the thermal and concentration gradients. These coefficients were functions of both the measured data and the calculated results, and the relationships are shown in equations (18)–(21). For the vapor flux equation, the parameter associated with the thermal gradient was the phenomenological coefficient, L_{vq}, divided by the absolute temperature squared, as shown in equation (10). This parameter varied from about 4×10^{-10} to 4×10^{-9} kg $m^{-1}\ s^{-1}\ K^{-1}$ with most of the runs averaging around 2×10^{-9} kg $m^{-1}\ s^{-1}\ K^{-1}$. The parameter for the concentration gradient was the phenomenological coefficient, $L_{vl}+L_{vv}$, times the ratio of the gas constant, R, to the humidity fraction, H. This concentration parameter ranged from about 2×10^{-7} to 4×10^{-7} kg $m^{-1}\ s^{-1}$ and averaged around 2.5×10^{-7} kg $m^{-1}\ s^{-1}$. As can be seen, the concentration parameter was 100 times greater than that for the temperature, but this was partially offset by the fact that the temperature gradient was usually about 25 times greater than the concentration gradient. When these parameters were multiplied by

their respective gradients and summed, the total vapor flux was determined. The flux contributions due to concentration and thermal gradients were about 80% and 20%, respectively. The concentration seemed to have the greater effect on mass transfer in the vapor phase.

The same type of analysis can be done for the liquid flux equation. The phenomenological coefficients associated with the thermal and concentration gradients were L_{lq} and $(L_{ll}+L_{lv})$, as shown in equation (9). As with the vapor coefficients, the thermal coefficient was divided by the absolute temperature squared, and the concentration coefficient was multiplied times the gas constant divided by the humidity. The resulting thermal and concentration parameters averaged around 2.3×10^{-10} kg m^{-1} s^{-1} K^{-1} and 3×10^{-7} kg m^{-1} s^{-1}, respectively. It was interesting to note that the concentration parameters for the liquid and vapor were almost the same value; whereas, the thermal parameter for the vapor was 100 times greater than that for the liquid phase. When the parameters were multiplied by their respective gradients, the liquid-flux contribution due to the concentration gradient was almost 50 times greater than the contribution due to the thermal gradient. This seemed to indicate that concentration difference was the major driving force for the liquid mass transfer, even to a greater extent than for the vapor.

Transient

The analysis of the transient results was based on the assumption that the vapor is always in equilibrium with the liquid at each point in the sample at all times during the run. As was stated earlier, this is a valid assumption for relatively slow processes. Also, it is important that the relative humidity has reached its steady-state value for all readings. The sensors and instrumentation were tested prior to the initial run and were shown to reach steady state in 10–15 s. The supplier claims that steady state is achieved in 30–45 s. In either case, this was essentially an instantaneous reading for this system.

The first change to occur in the samples was the change in temperature. For all the runs, the temperature profile reached steady state after 1–2 h. However, the relative humidity required from 30 to 300 h to reach steady state with 60 h being the normal time span. The steady-state temperature profile was established two orders of magnitude faster than the relative humidity profile. Therefore, the temperature change acted as a step change even though it is experimentally impossible to achieve.

Once it was known that the temperature profile was established very quickly, some of the other transient properties of the system could then be analyzed. Figure 10 is a plot of the response of the four relative humidity sensors vs time for Run 11. In most of the runs, 90% of the relative humidity change occurs in the first 6 h (20,000 s) and slowly approaches steady state at about 60 h (200,000 s). The step change

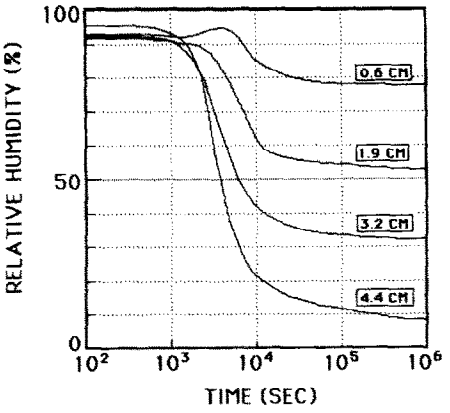

FIG. 10. Transient relative humidity response for average moisture content of 2.0%wt and temperature difference of 28.3°C.

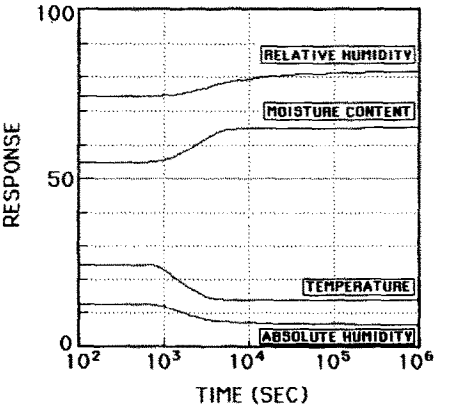

FIG. 11. Transient responses for an average moisture content of 0.6% wt and a temperature difference of 20.8°C at 0.6 cm.

response is that of a second order system with time delay (S-shaped curve). The most important observation is that most of the relative humidity change occurs very quickly with 90% of the total change occurring in the first 6 h.

The absolute humidities for all the runs were calculated at each of the four relative humidity sensors as a function of time. Again it was obvious that most of the change occurred in the first 6 h of the run. This is expected since this value was calculated based on the relative humidity and temperature readings. The absolute humidity profile was established in the same amount of time required to establish the relative humidity profile implying that absolute humidity is a strong function of relative humidity and a weaker function of temperature. However, the moisture content changed more quickly than the absolute humidity, about 1–2 h. This indicates that moisture content is a stronger function of temperature than it is a function of relative humidity, since the moisture content changes occur on the same time scale as the temperature changes.

It was interesting to note that Runs 5 through 11,

which all have an average moisture content of 2.0% wt, have a unique response of the relative humidity sensor nearest the cold plate (probe No. 1 at 0.6 cm). As the temperature profile was established, the moisture migrated rapidly toward the cold region, and the relative humidity near the cold plate initially increased as the moisture moved past the sensor toward the cold plate. This also shows that for the high average humidity at steady state, the majority of the moisture is stored near the cold plate. Therefore, although the steady-state relative humidity measurements do not show the effect of average moisture content, the transient response does show to some extent the effect of average moisture content.

Finally, Fig. 11 shows the temperature, relative humidity, moisture content and absolute humidity of probe No. 1 (0.6 cm) in the sample during Run 1. This graph shows the temperature, relative humidity, absolute humidity, and moisture contents changing simultaneously at one point in the sample. Reviewing the figures helps to show how all the responses are interrelated.

CONCLUSIONS

The relative humidity probes and thermocouples were used within the sample to directly measure relative humidity and temperature. The steady-state temperature and relative humidity gradients were found to be approximately linear in the hygroscopic moisture range. Using the measurement data, the moisture content, absolute humidity, vapor flux (which equals the liquid flux), and vapor and liquid mass conductivities were also calculated at each point for all 11 runs. The results were evaluated with respect to three variables: average temperature, temperature difference, and average moisture content. The concentration gradient, as opposed to the thermal gradient, was the major driving forces for both the liquid and vapor phases. The concentration contribution was about 98% of the total liquid flux and about 80% of the vapor flux. The results can be applied to current drying theory for use in the prediction of drying rates and conditions.

Acknowledgements—The authors would like to gratefully acknowledge the National Science Foundation for financial support and Maureen Phelan for help in the data analysis.

REFERENCES

1. A. V. Luikov, Drying theory, *Gesenergoizdat* **10,** 125–138 (1950).
2. A. V. Luikov, *Heat and Mass Transfer in Capillary Porous Bodies*. Pergamon Press, Oxford (1966).
3. A. V. Luikov, Systems of differential equations of heat and mass transfer in capillary—porous bodies (review), *Int. J. Heat Mass Transfer* **18,** 1–14 (1975).
4. E. R. G. Eckert and M. Faghri, A general analysis of moisture migration caused by temperature differences in an uninsulated porous medium, *Int. J. Heat Mass Transfer* **23,** 1613–1623 (1980).
5. K. Masmoudi and M. Maalej, Water migration in the porous media, *7th Int. Heat Transfer Conference*, pp. 83–86 (1982).
6. M. Fortes and M. Okos, A non-equilibrium approach to transport phenomena in equilibrium—porous media, *Proc. First Int. Symposium on Drying*, pp. 100–109 (1978).
7. W. C. Thomas, G. P. Bal and R. J. Onega, Heat and mass transfer in a glass fiber roof insulating material, ASTM-STP 789, pp. 582–601 (1983).
8. M. Fortes and M. Okos, Heat and mass transfer in hygroscopic capillary extruded products, *A.I.Ch.E. Jl* **27,** 255–262 (1981).
9. C. L. D. Huang, Effects of heat flux on the migration of moisture in a cylindrical concrete tube, *7th Int. Heat Transfer Conference*, pp. 73–78 (1982).
10. D. V. Luu, Hygroscopic moisture behavior in fibrous material. M.S. thesis, Drexel University, Philadelphia, PA (1984).
11. S. R. DeGroot, *Equilibrium of Irreversible Processes*, 2nd edn. North-Holland, Amsterdam (1951).
12. P. H. Pallady and P. J. Hanley, Evaluating moist air properties, *Chem. Engng* 117–118 (29 October 1984).
13. J. Y. Baladi, Transient heat and mass transfer in soils. Ph.D. thesis, Purdue University, West Lafayette, IN (1975).

TRANSFERT DE MASSE HYGROSCOPIQUE THERMIQUEMENT INDUIT DANS UN MILIEU FIBREUX

Résumé—Une éprouvette en fibre de verre humide est utilisée pour étudier le transfert de masse d'eau produit par une différence de température. Les sondes d'humidité et les thermocouples sont implantés dans l'éprouvette et équipés d'une saisie continue des changements d'humidité relative et de température résultant de la migration d'humidité. On étudie les effets de la température moyenne, de l'importance du gradient thermique, du contenu moyen d'humidité. Les données sont analysées en utilisant une analogie au modèle de thermodynamique des mécanismes irréversibles. Les flux de vapeur et de liquide sont évalués avec les conductivités de vapeur et de liquide. Les coefficients phénoménologiques associés aux flux massiques dus aux gradients de température et de concentration sont déterminés pour des conditions de régime permament. Des données transitoires pour humidité et température sont aussi mesurées ou calculées.

THERMISCH INDUZIERTER MASSENTRANSPORT IN EINEM FASERARTIGEN MATERIAL

Zusammenfassung—In einer Fiberglas-Probe wird der hygroskopische Massentransport untersucht, der durch einen Temperaturunterschied in feuchtem faserartigem Material hervorgerufen wird. Feuchtesonden und Thermoelemente wurden in die Rohre eingesetzt und zur kontinuierlichen Überwachung der Änderung von relativer Feuchte und Temperatur infolge der Feuchtigkeitswanderung verwendet. Der Einfluß der mittleren Temperatur, die Größe des Temperatur-Gradienten und des mittleren Feuchtegehaltes sind einige der untersuchten Parameter. Die Daten wurden mit einer mechanischen Analogie zum irreversiblen thermodynamischen Modell untersucht. Gas- und Flüssigkeitsströmungen wurden zusammen mit den entsprechenden Wärmeleitfähigkeiten für Gas und Flüssigkeit ermittelt. Die phänomenologischen Koeffizienten der Flüssigkeits- und Gasströmungen wurden berechnet und die Strömungsverteilung infolge von Temperatur- und Konzentrationsgradienten für den stationären Fall bestimmt. Die instationären Daten für Temperatur und Feuchtegehalt wurden entweder gemessen oder berechnet.

ГИДРОТЕРМИЧЕСКИЙ МАССОПЕРЕНОС В ВОЛОКОННЫХ СРЕДАХ

Аннотация—Для изучения гидротермического массопереноса, вызванного разностью температур поперек влажной волоконной среды, использовался образец из стекловолокна. Датчики влажности и термопары были введены в образец и служили для контроля за изменениями относительной влажности и температуры, вызванными миграцией влаги. Параметрами, влияние которых изучалось, были осредненная температура, величина теплового градиента и осредненного влагосодержания. Данные анализировались с использованием механистической аналогии модели термодинамики необратимых процессов. Потоки пара и жидкости оценивались одновременно с коэффициентами переноса пара и жидкости. Рассчитаны феноменологические коэффициенты, связанные с потоками жидкости и пара, и вклады в поток, обусловленные тепловыми и концентрационными градиентами для стационарного режима. Данные для нестационарных влажности, температуры и влагосодержания бали также либо измерены, либо рассчитаны.